Journal of Fluids and Structures (2001) **15,** 445–457
doi:10.1006/jfls.2000.0344, available online at http://www.idealibrary.com on IDEAL®

HYSTERESIS IN THE FORCED STUART–LANDAU EQUATION: APPLICATION TO VORTEX SHEDDING FROM AN OSCILLATING CYLINDER

P. Le Gal

Institut de Recherche sur les Phénomènes hors Equilibre
49, rue Frédéric Joliot-Curie, B.P. 146, F-13384 Marseille, Cedex 13, France

A. Nadim

Department of Aerospace and Mechanical Engineering, Boston University
Boston, MA 02215, U.S.A.

AND

M. Thompson

Department of Mechanical Engineering, Monash University
Clayton, VIC 3800, Australia

(Received 3 October 2000, and in final form 6 November 2000)

The complex Stuart–Landau equation models a prototypical Hopf bifurcation in which, when the control parameter exceeds a critical value, the null solution bifurcates into a finite amplitude time-periodic solution. We study the response of this equation to time-harmonic forcing in the subcritical regime (i.e., before the bifurcation). We show that when a second parameter in the Stuart–Landau equation passes a critical value, a portion of the solution surface as a function of forcing frequency and amplitude becomes multivalued. For instance, at a fixed forcing amplitude, one finds a well-defined range of frequencies over which two stable periodic responses may coexist, having different amplitudes. We apply this result to predict the behaviour of the wake downstream of an oscillating cylinder, and compare the predictions with experimental and computational observations of such a wake.

1. INTRODUCTION

The complex Stuart-Landau equation has been widely used to model the shedding of vortices in the two-dimensional wake of a cylinder at low Reynolds numbers. Specifically, the different coefficients of the model have been measured from experiments (Sreenivasan *et al.* 1986; Provansal *et al.* 1987; Schumm *et al.* 1994; Albarède & Provansal 1995) and from numerical simulations (Dušek *et al.* 1994). Two-dimensional flows past a laterally oscillating cylinder have also been the subject of extensive research. In particular, the experiments of Bishop & Hassan (1964) have clearly shown jumps and hysteresis loops in the resonance curves for the amplitude and the phase of the vortex shedding. These resonances appear for particular excitation frequencies, and Stansby (1976) has shown the existence of resonant horns where the wake is locked to the cross-flow oscillation of the cylinder. Different modes of vortex shedding can be associated with these lockings (Williamson & Roshko 1988); in particular, the classical Bénard–von Kármán wake can be excited among other nonsymmetric wakes. Visualization of moderate Reynolds number

0889–9746/01/040445 + 13 $35.00/0

forced wakes shows a jump in the phase of the vortex shedding when the frequency of the excitation passes through the resonance frequency (Ongoren & Rockwell 1988). The different phase lags between the laterally oscillating cylinder and the vortex shedding have been associated with a competition between several mechanisms of vorticity generation (Blackburn & Henderson 1999).

The present study is devoted to the theoretical analysis of the response of the forced Landau equation and to the comparison of its predictions with experiments and numerical simulations. We focus our attention on the subcritical regime, where the periodic solution is damped when it is not excited. To our knowledge, the only attempt at modelling the periodically forced wake by a forced Landau equation below the threshold has been by Provansal *et al.* (1987). In this case, the forcing term which is added to the model is a simple harmonic term, having a given amplitude and frequency. Above the threshold, additional third-order terms are involved in the amplitude equation associated with the forced Hopf bifurcation (Walgraef 1997). The solution is much more intricate in this case with the possibility of the appearance of higher-order resonances and biperiodic behaviour. A complete mathematical analysis of the different possibilities has been provided by Gambaudo (1985). In addition, numerical solutions of the forced Stuart–Landau equation in the supercritical regime have been obtained (Olinger 1993) to establish that its underlying dynamics are similar to those of the circle map.

In our work, we restrict our analysis to the subcritical regime of the Stuart–Landau equation where locking is expected (Gambaudo 1985). We find that, due to the cubic nonlinearity of the Landau equation, the resonance curve can exhibit a hysteresis loop in a certain range of parameters. This behaviour is similar to the response of a forced harmonic mechanical pendulum (Landau & Lifshitz 1976). We then compare our predictions against experiments and numerical simulations. In both cases, we study the two-dimensional wake of a circular cylinder subject to cross-flow oscillations. Although the predicted resonance below the Bénard–von Kármán threshold is observed, no evidence of hysteretic behaviour has yet been seen in the experiments and computations.

2. THE FORCED STUART–LANDAU EQUATION

The complex Stuart–Landau equation with time-periodic forcing is given by

$$\frac{\mathrm{d}A}{\mathrm{d}t} = (a_R + \mathrm{i}a_I)A - \ell_R(1 + \mathrm{i}c)|A|^2A + F\mathrm{e}^{\mathrm{i}\omega t}, \tag{1}$$

in which A is a complex-valued function of time t and the parameters a_R, a_I, ℓ_R ($\ell_R > 0$) and c are all real. The last term in this equation represents the forcing. We take the forcing amplitude F and frequency ω to be real.

In the absence of forcing, equation (1) represents the normal form of the Hopf bifurcation which occurs at the critical value of the parameter $a_R = 0$. For $a_R < 0$, the null solution $A = 0$ is a stable solution of the unforced equation. For $a_R > 0$, this base state loses its stability and the solution settles down to a time-periodic state with constant amplitude $|A| = (a_R/\ell_R)^{1/2}$, orbiting the origin in the complex plane with angular velocity $a_I - a_Rc$. Note that parameter ℓ_R is taken to be positive. The time-scale for the transient approach to this final periodic state is given by a_R^{-1}.

In order to investigate the forced response of the system, we first non-dimensionalize equation (1) so as to minimize the total number of parameters that need to be studied. Using the natural scales of the system which are evident in the supercritical solution just discussed,

and subtracting the constant rotation imparted by parameter a_I, we define the following dimensionless (primed) variables:

$$t' \equiv |a_R|\, t, \tag{2}$$

$$A'(t') \equiv (\ell_R/|a_R|)^{1/2} A(t)\, \mathrm{e}^{-\mathrm{i}a_I t}, \tag{3}$$

$$F' \equiv |a_R|^{-1} (\ell_R/|a_R|)^{1/2} F, \tag{4}$$

$$\omega' \equiv (\omega - a_I)/|a_R|. \tag{5}$$

Upon substitution into equation (1) we obtain

$$\frac{\mathrm{d}A'}{\mathrm{d}t'} = \mathrm{sgn}(a_R)\, A' - (1 + \mathrm{i}c)\, |A'|^2 A' + F' \mathrm{e}^{\mathrm{i}\omega' t'},$$

in which $\mathrm{sgn}\,(a_R)$ is the sign of the Hopf bifurcation parameter a_R. In what follows, we shall focus our attention on the forced response of the subcritical state $a_R < 0$. This corresponds to the vortex shedding experiments and simulations which are also being reported in Sections 3 and 4 of this paper. The supercritical case exhibits a much richer (and more difficult to analyse) variety of solutions; see Gambaudo (1985) for a detailed discussion. Considering the subcritical case $a_R < 0$ only, we rewrite the last equation and drop the primes from all the variables for clarity to obtain

$$\frac{\mathrm{d}A}{\mathrm{d}t} = -A - (1 + \mathrm{i}c)\, |A|^2 A + F \mathrm{e}^{\mathrm{i}\omega t}. \tag{6}$$

Three real dimensionless parameters, c, F and ω, entirely determine the solution $A(t)$. Parameter c is an intrinsic property of the unforced system; for the supercritical state, it would determine the frequency of the solution after the Hopf bifurcation. Parameters F and ω are simply the amplitude and reduced frequency of the time-periodic forcing. In the following, we restrict our attention to the case $F > 0$. The case of negative F is identical, but with a corresponding sign change in A (i.e., with a phase difference of π).

2.1. Phase-Locked Solution

To obtain two real equations from the complex equation (6), we first write $A(t)$ in the form

$$A(t) = \rho(t)\, \mathrm{e}^{\mathrm{i}\phi(t)},$$

where $\rho(t) = |A(t)|$ is the real and nonnegative amplitude of the complex function A and $\phi(t)$ is its phase (also real). Substitution into equation (6) results in the pair of equations

$$\dot{\rho}/\rho = -1 - \rho^2 + (F/\rho)\cos(\omega t - \phi), \tag{7}$$

$$\dot{\phi} = -c\rho^2 + (F/\rho)\sin(\omega t - \phi), \tag{8}$$

in which the overdot represents the time derivative. We now seek a solution of constant magnitude whose phase is locked with the forcing, lagging behind it with constant angle ϕ_o. In other words, we seek a solution of the form $\rho = \rho_o$ and $\phi = \omega t - \phi_o$, where ρ_o and ϕ_o are constants. Such a solution would have to satisfy

$$0 = -1 - \rho_o^2 + (F/\rho_o)\cos\phi_o, \tag{9}$$

$$\omega = -c\rho_o^2 + (F/\rho_o)\sin\phi_o. \tag{10}$$

Upon elimination of ϕ_o between equations (9) and (10) (by collecting the trigonometric terms on one side, squaring and adding the two equations), a single algebraic equation for the amplitude ρ_o is readily obtained. Upon defining $x \equiv \rho_o^2$, this equation reads

$$x[(1+x)^2 + (\omega + cx)^2] = F^2, \tag{11}$$

which is cubic in x, with its solution depending on the three parameters, c, F and ω, of the original system. Of course, the only solutions which are acceptable are real and non-negative. Furthermore, once a solution $x = \rho_o^2$ has been found, the phase-lag ϕ_o can always be obtained by solving

$$\tan \phi_o = \frac{\omega + cx}{1+x}. \tag{12}$$

Being a cubic equation with real coefficients, equation (11) may have up to three real solutions, depending upon the parameters of the system. The parameter ranges for which three real and positive solutions exist are of particular interest, since they suggest the possibility of having multiple states of the system under identical forcing conditions. Fortunately, equation (11) is simple enough that a complete analysis as a function of the three independent parameters c, F and ω is possible; this is what we now attempt.

Denote the left-hand side of equation (11) by $g(x; c, \omega)$, i.e.,

$$g(x; c, \omega) \equiv x[(1+x)^2 + (\omega + cx)^2]. \tag{13}$$

The amplitude of the phase-locked solution is thus obtained from the positive solutions x to $g(x) = F^2$. Graphically, this can be achieved by plotting the function $g(x)$ (for a given set of parameters c and ω) over positive x and considering the intersections of this graph with horizontal lines which are drawn at height F^2 above the x-axis. As it turns out, the cubic function $g(x)$ [which is asymptotic to $(1+\omega^2)x$ for small x and to $(1+c^2)x^3$ for large x] can only have one of the two forms depicted in Figure 1. Namely, over the positive range of x, the function $g(x)$ is either monotonically increasing, as depicted in Figure 1(a), or it goes through a local maximum and minimum prior to increasing indefinitely as x increases, as drawn in Figure 1(b). In the latter case, there is clearly a pair of values, $F_{\min}$ and $F_{\max}$, such that for $F_{\min} < F < F_{\max}$, the equation $g(x) = F^2$ admits three positive solution for x.

To identify the region of the (c, ω) parameter space within which the function $g(x; c, \omega)$ has a shape similar to that in Figure 1(b), let us find the position of the local maximum and minimum of $g(x)$. These are found by setting

$$\frac{\partial g}{\partial x} = 3(1+c^2)x^2 + 4(1+c\omega)x + (1+\omega^2) = 0. \tag{14}$$

As such, the local extrema are located at

$$x_\pm = \frac{-2(1+c\omega) \pm \sqrt{4(1+c\omega)^2 - 3(1+c^2)(1+\omega^2)}}{3(1+c^2)}. \tag{15}$$

Evidently, in order that both x_- and x_+ be positive, i.e. to have a local maximum and minimum in $g(x)$ over positive x, we must require that

$$-2(1+c\omega) > 0, \tag{16}$$

$$4(1+c\omega)^2 - 3(1+c^2)(1+\omega^2) > 0. \tag{17}$$

Condition (16) requires $c\omega < -1$ which means that ω and c must be of different signs and the magnitude of ω must be larger than $|c|^{-1}$. Simultaneously, condition (17) must be met.

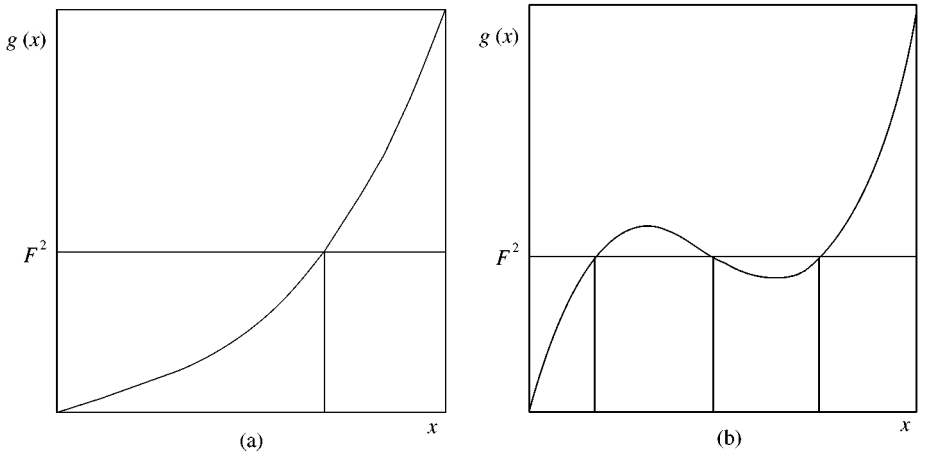

Figure 1. Possible shapes of the cubic function $g(x)$: (a) single solution to $g(x) = F^2$; (b) multiple solutions to $g(x) = F^2$.

The latter can be written as a quadratic function of ω in the form

$$(c^2 - 3)\,\omega^2 + 8c\omega + (1 - 3c^2) > 0. \tag{18}$$

To analyse the parameter space further, we now restrict our attention to the case $c < 0$. There are two reasons for doing so. First, parameter c for cylinder wakes is known to be negative. Secondly, since parameters c and ω appear throughout the above only in the forms ω^2, c^2 and $c\omega$, any statement which is true for a given pair of values (c, ω) is also true for the pair $(-c, -\omega)$. Therefore, the behaviour for positive c can be directly inferred from the results obtained for $c < 0$.

Based upon condition (16), for $c < 0$, multivalued solutions to $g(x) = F^2$ can only exist if $\omega > 0$. So, let us now consider the left-hand side (lhs) of condition (18) for positive ω. The coefficient of ω^2 determines whether the parabola obtained when this lhs is plotted against positive ω points upward or downward. There are three possibilities to explore: (i) When the coefficient $(c^2 - 3)$ is negative, i.e., for $-\sqrt{3} < c < 0$, the lhs of equation (18) monotonically decreases from $(1 - 3c^2)$ to $-\infty$, as ω goes from 0 to ∞. Even if this lhs starts out being positive at $\omega = 0$ [which is the case when $(1 - 3c^2) > 0$], it will eventually become negative as ω gets larger. Recalling that condition (16) required the magnitude of ω to exceed $|c|^{-1}$ in order to have multivalued solutions, it is easy to show that in this case, conditions (16) and (18) cannot be simultaneously satisfied and the solution to $g(x) = F^2$ is always single-valued. (ii) When the coefficient $(c^2 - 3)$ vanishes, i.e., when $c = -\sqrt{3}$, the lhs of equation (18) becomes a straight line when plotted against ω, and it is always negative for positive values of ω. Therefore, condition (18) cannot be satisfied and the solution to $g(x) = F^2$ remains single-valued. (iii) Finally, when the coefficient $(c^2 - 3)$ is positive, i.e., when $c < -\sqrt{3}$, the lhs of equation (18) starts out negative at $\omega = 0$, but it will eventually cross zero and remain positive as ω increases. Hence, condition (18) will be met for ω larger than a critical value (which is a root of the lhs, given explicitly below). In that range of ω, the first condition which required that $\omega > |c|^{-1}$ is also satisfied and, therefore, multivalued solutions to $g(x) = F^2$ can exist.

These results can be summarized as follows. In order for the cubic equation $g(x; c, \omega) = F^2$ to admit multivalued solutions for x, parameter c must satisfy $c < -\sqrt{3}$ and ω must be

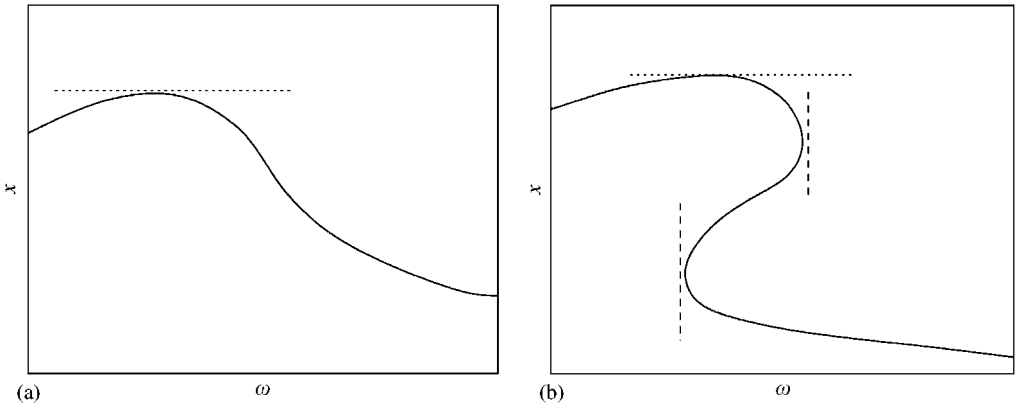

Figure 2. The frequency–response curves, x versus ω: (a) single-valued case, (b) multivalued case.

larger than the positive root (in ω) of the lhs of equation (18), i.e.,

$$c < -\sqrt{3} \quad \text{and} \quad \omega > \omega_{\text{crit}} \equiv \frac{\sqrt{3}\,c - 1}{c + \sqrt{3}}. \tag{19}$$

For any (c, ω) which satisfy conditions (19), the graph of the function $g(x)$ resembles Figure 1(b). There will then exist the pair of values

$$F_{\min} = \sqrt{g(x_+; c, \omega)} \quad \text{and} \quad F_{\max} = \sqrt{g(x_-; c, \omega)} \tag{20}$$

with $x_\pm$ given by equation (15), such that for $F_{\min} < F < F_{\max}$, the equation $g(x; c, \omega) = F^2$ possesses three positive solutions for the amplitude $x = \rho_o^2$. At exactly the critical value $\omega = \omega_{\text{crit}}$, i.e., just before multivalued solutions emerge, the corresponding critical forcing amplitude is given by

$$F_{\text{crit}}^2 = \frac{-8}{3\sqrt{3}} \frac{(c^2 + 1)}{(c + \sqrt{3})^3}.$$

2.2. Resonance

For a fixed forcing amplitude F, as the forcing frequency ω varies, the amplitude $\rho_o = \sqrt{x}$ of the phase-locked solution also varies. The graph obtained by plotting the response of the system (characterized by ρ_o or x) as a function of the forcing frequency ω is the frequency–response curve. Note that under the conditions described above, this curve may be multivalued over a certain range of frequencies. Let us now consider the problem of finding the forcing frequency at which the response has its largest amplitude. We define this as "resonance" for our nonlinear oscillator.

Equation (11) can be thought of as providing an implicit solution for the response x as a function of frequency ω for a fixed value of the forcing amplitude F. Typically, the frequency–response curves which result may resemble those in Figure 2, depicted here under the conditions when the solution is single-valued, [Figure 2(a)], or multivalued [Figure 2(b)].

In either case, the maximum in the curve (resonance) is obtained by finding the frequency at which the derivative $\partial x/\partial \omega$ vanishes. Given the implicit solution $g(x; c, \omega) = F^2$, for

constant values of parameters c and F, this derivative is found to be

$$\frac{\partial x}{\partial \omega} = -\frac{\partial g/\partial \omega}{\partial g/\partial x}. \tag{21}$$

The numerator $\partial g/\partial \omega$ is simply given by $2x(\omega + cx)$, indicating that resonance occurs when $\omega = -cx$. Therefore, at resonance, equation (11) reduces to

$$x_{\text{res}}(1 + x_{\text{res}})^2 = F^2. \tag{22}$$

Once the solution $x_{\text{res}}(F)$ to this equation is obtained, the resonance frequency as a function of forcing amplitude is given by

$$\omega_{\text{res}}(F) = -c\, x_{\text{res}}(F). \tag{23}$$

For large F the solution behaves as $x_{\text{res}} \sim F^{2/3}$, whereas for small F its behaviour is like $x_{\text{res}} \sim F^2$. More generally, the solution to the cubic equation (22) is given by

$$x_{\text{res}}(F) = \tfrac{1}{6} W^{1/3} + \tfrac{2}{3} W^{-1/3} - \tfrac{2}{3}, \tag{24}$$

where

$$W \equiv 8 + 108F^2 + 12(12F^2 + 81F^4)^{1/2}. \tag{25}$$

As such, for a fixed c, there is a well-defined resonance curve in the (ω, F)-plane over which resonance occurs and the amplitude ρ_o of the solution is a maximum. An explicit graph of this curve for a typical value of c will be presented in a later subsection.

Since at resonance, $\omega + cx = 0$, the phase-lag of the resonant solution is found from equation (12) to be $\phi_o = 0$ provided we take $F > 0$; note that besides satisfying (12), the phase-lag must also be consistent with $(F/\rho_o)\sin\phi_o = \omega + cx$ and $(F/\rho_o)\cos\phi_o = 1 + x$. Upon recalling that in the Stuart–Landau equation, the function A can be thought of as being proportional to "velocity" rather than "displacement", this behaviour is seen to be consistent with standard linear oscillators for which the displacement lags the forcing by a phase of $\pi/2$ while the velocity and the forcing are in phase at resonance.

We also make the observation that the points at which the denominator in equation (21) vanishes are where the derivative of the frequency–response curve becomes infinite. These points are identified by the vertical dashed lines in Figure 2(b). Evidently, having two such points is a prerequisite for having a range of frequencies over which the solution is triple-valued. The vanishing of this denominator is precisely the condition we posed earlier [cf. equation (14)] to locate a local maximum and minimum of $g(x)$ over positive x. It is also possible to demonstrate that in the multivalued frequency–response curve, [Figure 2(b)] the portion of the curve connecting the two turning points (tangent to the dashed vertical curves) is unstable, whereas the upper and lower segments of this curve are stable.

2.3. Results for $c = -3$

The small dimensionless parameter c in the Stuart–Landau equation describing the wakes of cylinders has been measured for cylinders of different aspect ratios. For an aspect ratio of 10, its value turns out to be approximately $c = -3$ (Albarède *et al.* 1995; Peschard 1995). The experimental portion of this work deals with subcritical uniform flow past a cylinder of aspect ratio 10; therefore, let us consider more precisely the nature of the solution at $c = -3$.

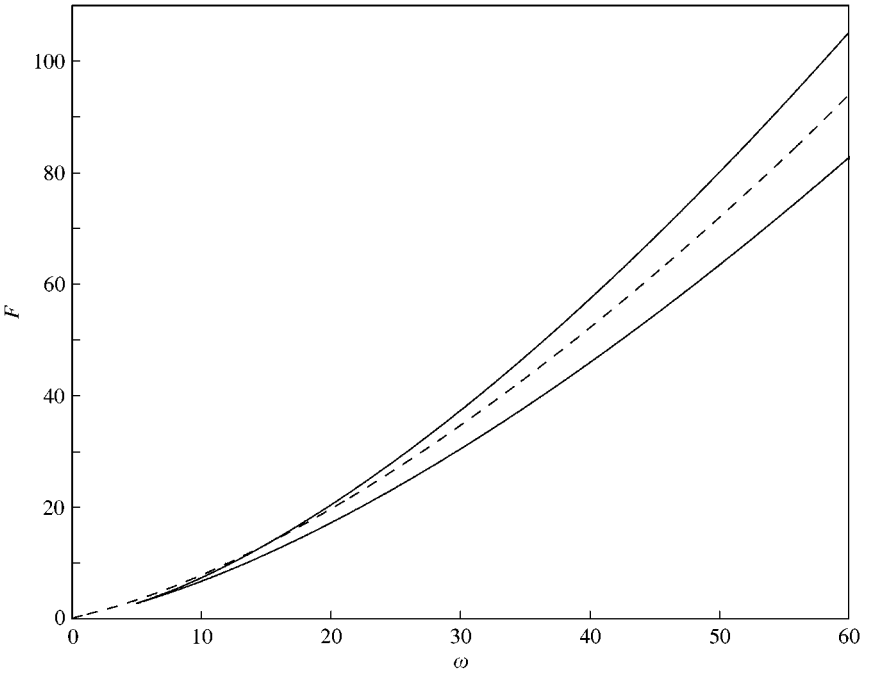

Figure 3. The minimum and maximum values of F (solid lines) which bound the region in which the solution is multivalued for $c = -3$. The dashed line represents the resonance curve at $c = -3$.

Since this value of c is less than the critical value $-\sqrt{3}$, we know that for large enough frequencies, we will always have a window of forcing amplitudes over which multivalued solutions exist. The critical value ω_{crit} which needs to be exceeded is given by equation (19) and turns out to be $\omega_{\text{crit}} \approx 4{\cdot}8868$. The corresponding critical value of the forcing at this point turns out to be $F_{\text{crit}} \approx 2{\cdot}7482$. For any ω larger than ω_{crit}, there exist lower and upper bounds F_{min} and F_{max}, given by equation (20), such that for values of F which are in between, the solution surface is multivalued. In the (ω, F)-plane, we can trace out the two curves which provide the bounds on F as a function of ω. We have done this in Figure 3 for $c = -3$. The two solid lines which form a cusp at the critical point $(\omega_{\text{crit}}, F_{\text{crit}}) = (4{\cdot}8868, 2{\cdot}7482)$ in this figure represent these bounds.

Also in Figure 3, we have traced out the resonance curve given by equations (22), (23) and (25), for the case $c = -3$. The resonance curve enters the multivalued region as ω and F increase and remains there. That is, the maximum point in Figure 2(b) lies somewhere in between the two turning points with infinite slopes (when ω and F are large enough). Lastly, we show in Figure 4, the solution surface itself ($\rho_o = \sqrt{x}$ versus ω and F) for $c = -3$ obtained by plotting a family of solutions at different frequencies as the forcing amplitude is varied. It is clear that surface is folded and above the region bounded by the solid curves in Figure 3, the solution is triple-valued. Of the three solutions, those with the largest and smallest amplitudes are stable while the one in the middle is unstable.

3. EXPERIMENTAL OBSERVATIONS

As explained before, the parameter c is a constant which characterizes the limit cycle which appears at the Hopf bifurcation. For the Bénard–von Kármán wake, it has been measured

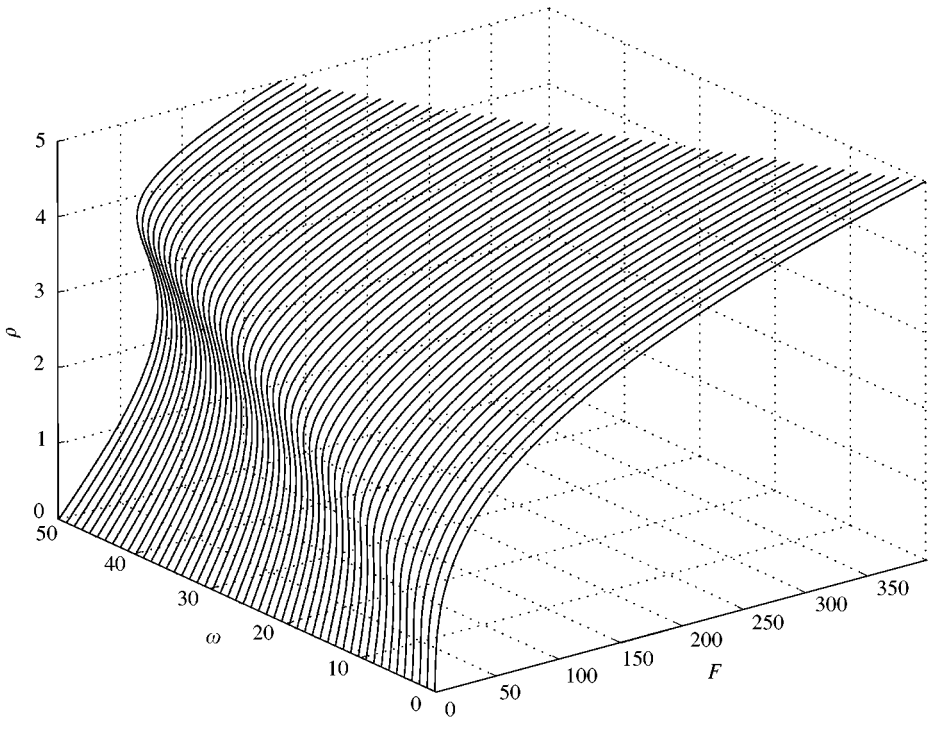

Figure 4. The solution surface $\rho_o(\omega, F)$ at $c = -3$.

both experimentally and numerically. However, this value varies with the aspect ratio of the cylinder that generates the wake. In our experiments, the cylinder has a diameter of 2 mm and a length of 20 mm, giving an aspect ratio of 10 which, according to Peschard (1995) and Albarède *et al.* (1995) gives a value for c close to -3. In this case, the critical Reynolds number for the appearance of the vortex street is about 70. The flow is generated in a water tunnel and the cylinder is mounted on a support which can oscillate at a given frequency by the use of an electric motor. In this study, only visual observations will be reported. These visualizations are made by oxidation of a tin wire. As predicted by our theoretical analysis, a strong resonance is seen when the forcing frequency is close to the natural frequency of the wake. Figure 5 presents snapshots of the wake for different cross-flow oscillation frequencies and for a Reynolds number equal to 60. On these images, the amplitude of the cylinder oscillation is 3 mm (the corresponding nondimensional value for F is not known *a priori* because we do not know how much energy is actually transmitted to the wake when oscillating the cylinder). The resonance phenomenon is clearly evidenced by the shedding of strong vortices when the excitation frequency approaches a value close to 1 Hz. In the figure caption, we also indicate the values of the non-dimensional frequency calculated using the expected parameters of the Landau equation [see Peschard (1995), Olinger (1993)]. Scanning the forcing frequency up and down does not reveal (at least visually) any hysteretic behaviour. More experiments would seem to be necessary to confirm this apparent deviation from the Landau model prediction. Let us note in particular that the strong spatial deformation of the wake, as it is visualized in Figure 5, is not taken into account in the model. This effect might be avoided when applying a very weak forcing very close to the threshold where the receptivity of the wake is large.

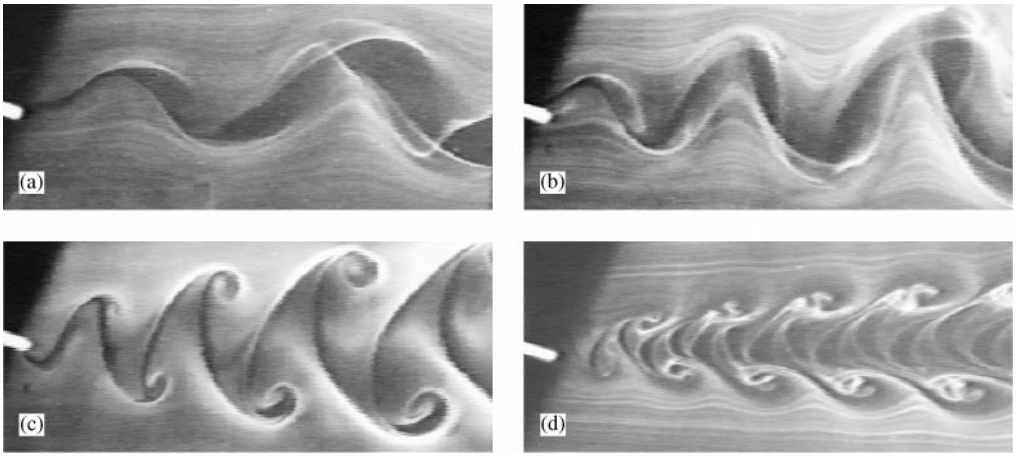

Figure 5. Visualization of the wake at Re = 60 for different exciting frequencies: (a) 0·52 Hz ($\omega = -10$); (b) 0·70 Hz ($\omega = -7$); (c) 0·95 Hz ($\omega = -2{\cdot}4$); (d) 1·4 Hz ($\omega = 5{\cdot}6$).

4 NUMERICAL SIMULATIONS

Two-dimensional numerical simulations were also undertaken to explore the frequency response. These were done with a spectral-element code described in Thompson *et al.* (1996), which employs a similar method to that used to examine the unforced post-transition behaviour in Dušek *et al.* (1994). Initial runs were performed to verify the chosen domain size and mesh point distribution and density were adequate.

The system was forced by applying an oscillating cross-flow velocity at the inlet and side boundaries of the domain, i.e., at the inlet and side boundaries $\mathbf{u} = (1, (B/\omega)\sin(\omega t))$. The cross-flow amplitude is divided by ω to maintain a constant acceleration forcing amplitude as dictated by the Landau model. It is thus expected that there is a linear relationship between B and F regardless of frequency. Note that in the numerical simulations, the governing equations are rendered dimensionless using the diameter of the cylinder as the length scale and the ratio of that diameter to the uniform flow velocity as the time scale.

Initially, runs were performed to determine the values of the critical parameters in the Landau model. Simulations at Re = 50, 48 and 45, the first two starting from the two-dimensional steady flow and the last from the time-periodic flow at Re = 48, allowed the transition Reynolds number to be determined as $\mathrm{Re}_{\mathrm{crit}} = 46{\cdot}7$ from interpolation of the measured growth rates. The dimensionless Landau constant was also evaluated for Re = 50 and 48 by determining the difference between the frequency of oscillation in the linear regime and at saturation. As in Dušek *et al.* (1994), the response was monitored by the vertical velocity at various points in the domain. For these two cases, the Landau constant was determined to be $c(\mathrm{Re} = 50) = -2{\cdot}52$ and $c(\mathrm{Re} = 48) = -2{\cdot}78$. Thus, it is less than the critical value of $c_{\mathrm{crit}} = -\sqrt{3}$ from the theoretical analysis [equation (19)] in this paper and consistent with estimates from Dušek *et al.* (1994). To examine the response in the subcritical regime, simulations were performed at Re = 44. At this Reynolds number, the model parameters (scaled with the time-scale mentioned above) can be estimated by extrapolation to be $a_I = 0{\cdot}3648$, $a_R = -0{\cdot}0057$, $c = -3{\cdot}3$ and $l_R = 0{\cdot}32$. Again, the critical parameter is the Landau constant, c, which indicates that the system should be hysteretic if the forcing is above a critical value. The frequency response was determined numerically by fixing the forcing level and stepping up from one forcing frequency to another after the

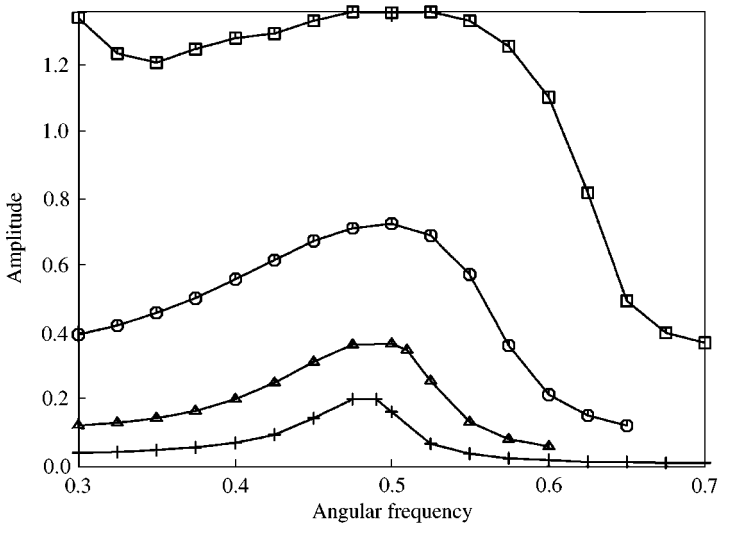

Figure 6. Numerical resonance curves for forcing amplitudes (B) of 0·01 (crosses), 0·03 (triangles), 0·10 (circles) and 0·30 (squares). The Reynolds number is 44. The curves show the amplitude of the vertical velocity component on the centreline 4 radii downstream of the cylinder centre.

Figure 7. Vorticity plots of the oscillating wake. The forcing amplitude is set to 0·01. The centre plot shows the response at close to the optimal forcing frequency. The top and bottom plots show the wake for forcing frequencies 25% below and 25% above the resonant frequency, respectively.

periodic asymptotic solution had been reached. This response is shown in Figure 6 for forcing amplitude $B = 0{\cdot}01$, 0·03, 0·10 and 0·30. These curves show the amplitude of the vertical velocity component at a point 4 radii downstream from the cylinder centre on the

symmetry axis. The nonlinear shift of the maxima, as predicted by equation (23) and observed in the experiments, is visible. Note that the sign of this deviation (here towards higher frequencies) is opposite to that of parameter c in agreement with predictions. Although the shift is in the right direction, it does not show the expected quadratic behaviour predicted by equation (23) for low forcing amplitudes.

Figure 7 shows the wake vorticity pattern corresponding to forcing (from top to bottom) at 25% below, equal to, and 25% above the resonant frequency. The asymmetry of the response—characteristic of the presence of odd terms in the dynamical system—is again evident through these visualizations; however, no hysteresis is observed.

5. CONCLUSION

The mismatch between both the experimental and numerical results, and the theoretical analysis, is surprising. The study of Dušek *et al.* (1994) indicates that the post-transition behaviour obeys the unforced Landau equation to a high degree of accuracy. One possible explanation is that higher-order terms in the Landau equation are not necessarily small and may contribute to the saturated behaviour. This is suggested by the failure of the numerical frequency–response curves to conform to the predictions of equation (23). If quintic and higher-order terms cannot be neglected in equation (1), they will cause deviations from the current predictions; preliminary numerical studies indicate that the predicted hysteresis can easily be destroyed by the additions of such terms. Moreover, the value of c in the numerical simulations was estimated indirectly based on the observed amplitude and frequency at saturation; hence it relies on the higher-order terms being negligible.

Because the scaled critical value of F only depends on c, equations (3) and (4) suggest that the dimensional critical forcing and the response amplitude both approach zero as the Reynolds number approaches the transition value. In turn, this means that close to the critical Reynolds number there should be some range of forcing for which high-order terms can be neglected and hysteresis will occur, provided $c < -\sqrt{3}$. The numerical results suggest that this range may be very small. Unfortunately, close to the transition Reynolds number, and for very small forcing amplitudes, it takes many cycles for the transient response to decay and hence it is difficult to explore this region numerically. We are currently attempting to obtain direct measures of the critical parameters of the Landau model to further refine the predicted behaviour (if necessary including the effects of higher-order terms). It will then be possible to better test the validity of the model by careful comparisons with the numerical frequency–response curves. These results will be reported elsewhere.

REFERENCES

ALBARÈDE, P. & PROVANSAL, M. 1995 Quasi-periodic cylinder wakes and the Ginzburg–Landau model. *Journal of Fluid Mechanics* **291,** 191–222.

BISHOP, R. E. D. & HASSAN, A. Y. 1964 The lift and drag forces on a circular cylinder oscillating in a flowing fluid. *Philosophical Transactions of the Royal Society (London)* A **227,** 51–75.

BLACKBURN, H. M. & HENDERSON, R. D. 1999 A study of two-dimensional flow past an oscillating cylinder. *Journal of Fluid Mechanics* **385,** 255–286.

DUŠEK, J., LE GAL, P. & FRAUNIÉ, P. 1994 A numerical and theoretical study of the first Hopf bifurcation in a cylinder wake. *Journal of Fluid Mechanics* **264,** 59–80.

GAMBAUDO, J. M. 1985 Perturbation of a Hopf bifurcation by an external time-periodic forcing. *Journal of Differential Equations* **57,** 172–199.

LANDAU, L. D. & LIFSHITZ, E. M. 1976 *Mechanics*, 3rd edition. Oxford: Pergamon Press.

Olinger, D. J. 1993 A low-dimensional model for chaos in open fluid flows. *Physics of Fluids* A **5,** 1947–1951.

Ongoren, A. & Rockwell, D. 1988 Flow structure from an oscillating cylinder. Part 1. Mechanisms of phase shift and recovery in the near wake. *Journal of Fluid Mechanics* **191,** 197–223.

Peschard, I. 1995 De l'oscillateur aux sillages couplés. Ph.D. Thesis, Université de la Méditerranée, Marseille, France.

Provansal, M., Mathis, C. & Boyer, L. 1987 Bénard–von Kármán instability: transient and forced regimes. *Journal of Fluid Mechanics* **182,** 1–22.

Schumm, M., Berger, E. & Monkewitz P. A. 1994 Self-excited oscillations in the wake of two-dimensional bluff bodies and their control. *Journal of Fluid Mechanics* **271,** 17–53.

Stansby, P. K. 1976 The locking-on vortex shedding due to the cross-stream vibration of circular cylinders in uniform and shear flows. *Journal of Fluid Mechanics* **74,** 641–655.

Sreenivasan, K. R., Strykowski, P. J. & Olinger, D. J. 1986 Hopf bifurcation, Landau equation, and vortex shedding behind circular cylinders. In *Proceedings of the Forum on Unsteady Flow Separation* (ed. K. N. Ghia). FED-Vol. 52, pp. 1–13, New York: ASME.

Thompson, M. C., Hourigan, K. & Sheridan, J. 1996 Three-dimensional instabilities in the wake of a circular cylinder. *Experimental Thermal and Fluid Science* **12,** 190–196.

Walgraef, D. 1997 *Spatio-Temporal Pattern Formation*: *with Examples from Physics*, *Chemistry and Materials Science*. Berlin: Springer Verlag.

Williamson, C. H. K. & Roshko, A. 1988 Vortex formation in the wake of an oscillating cylinder. *Journal of Fluids and Structures* **2,** 355–381.